Electronic Supplementary Material (ESI) for Nanoscale.

Strains and Defects Engineered Monolayer Ni-MoS_2 for pH-universal Hydrogen Evolution Catalysis

Dan Liang[a,b], Yong-Wei Zhang[b], Pengfei Lu[a,*], Zhi Gen Yu[b,**]

[a]*State Key Laboratory of Information Photonics and Optical Communications, Beijing University of Posts and Telecommunications, Beijing 100876, China*

[b]*Institute of High Performance Computing, A*STAR, Singapore 138632, Singapore*

[*]To whom correspondence should be addressed. E-mail: photon.bupt@gmail.com

[**]To whom correspondence should be addressed. E-mail: yuzg@ihpc.a-star.edu.sg

Supporting information

This file includes:

Computational methods

Our theoretical calculations were based on the density functional theory (DFT)[1] as implemented in the Vienna *ab-initio* Simulation Package (VASP).[2,3] We used the projector augmented wave method (PAW)[4,5] to represent electron-ion interactions, and the Perdew-Burke-Ernzerhof (PBE) functional within the generalized gradient approximation (GGA)[6] was considered for exchange correlation interactions. In addition, the vdW-DF2 method was used to describe the van der Waals interaction.[7-10] The energy cutoff for the plane-wave basis set was chosen to be 500 eV. The structures were relaxed until the forces on each atom were less than 0.01 eV/Å and the maximum energy change was of the order of 10^{-6} eV. To prevent interaction between two neighboring surfaces, a vacuum slab of 15 Å was employed in *z*-direction. The spin-polarization was considered in this work. The energy barriers for Heyrovsky, Tafel mechanism and water dissociation were determined using climbing image nudged elastic band (NEB) calculations.[11] The Gibbs free energy (ΔG_H) of the basal planes for both perfect and S vacancy-contained Ni-MoS_2 was calculated using supercells containing 4×4 and 6×6 unit cells, respectively. The *k*-points for the first Brillouin zone were sampled on a mesh grid of 4×4×1 and 2×2×1 for 4×4 and 6×6 supercells, respectively. In order to determine the dynamic stability of Ni-MoS_2, we calculated the phonon spectrum based on the force constant approach using the software package Phonopy.[12] Finite temperature analysis of the system at 1200K was conducted through *ab-initio* molecular dynamics (AIMD). The AIMD simulations were performed using 3000 time steps with a 0.5 fs time step at 1200 K. We employed non-self-consistent G_0W_0 correction[13] for MoS_2 to calculate the bandgap, and compare the PBE and GW bandgap energies. G_0W_0 correction accounts for the many-body electron interactions but retains the input PBE wave functions, thus results in the more accurate bandgap. A unified *k*-point mesh 12×12×1 is adopted for the G_0W_0.

The adsorption energy (ΔE_H) is computed as[14]

$$\Delta E_H = E(*H) - E(*) - \frac{1}{2}E(H_2) \quad (1)$$

where E(*H) and E(*) are the total energy of a supercell with and without hydrogen adsorption, respectively, and $E(H_2)$ is the total energy of a H_2 molecule.

The Gibbs free energy of H (ΔG_H) is defined as:

$$\Delta G_H = \Delta E_H + \Delta E_{ZPE} - T\Delta S_H \qquad (2)$$

where ΔE_{H} is the adsorption energy, ΔE_{ZPE} is the difference in zero-point energy, T is the temperature (300 K) and ΔS_H is the entropy difference between H that is adsorbed and in the gas phase. We approximated the entropy of hydrogen adsorption as $\Delta S_H \approx \frac{1}{2}(S^{\circ}_{H_2})$, where $S^{\circ}_{H_2}$ is the entropy of gas phase H_2 at standard conditions. Therefore, the correction factor of $(\Delta E_{ZPE} - T\Delta S_H)$ was computed to be 0.223 eV in this study.

Table S1. Calculated values of lattice parameter (a), bond length ($d_{\mathrm{M\text{-}S}}$, M=Mo,Ni) for MoS_2, NiS_2, Ni-MoS_2, respectively, and formation energy (E_{f}) of Ni-MoS_2.

	a (Å)	$d_{\mathrm{M\text{-}S}}$ (Å)	E_{f}(eV)
MoS_2	3.192, 3.160[15]	2.41, 2.42[15]	
NiS_2	3.54, 3.40[16]	2.58, 2.24[16]	
Ni-MoS_2	3.351	2.418 (Mo-S) 2.279 (Ni-S) 3.857 (*Ni-S)	-1.222

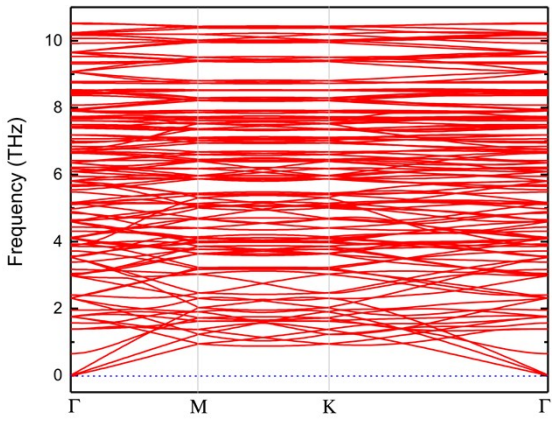

Figure S1. Calculated phonon-dispersion curves of Ni-MoS_2 along major symmetry directions of the Brillouin zone.

Table S2. Mechanical properties of Ni-MoS_2, MoS_2 and NiS_2 predicted by first-principles calculations.

	Stiffness Tensor (N/m)	Youngs's Modulus (N/m)	Shear Modulus (N/m)	Poisson's Ratio
Ni-MoS_2	C_{11} = 93.545 C_{22} = 62.575 C_{12} = 16.019 C_{66} = 16.694	Y_x = 89.444 Y_y = 59.832	Y_y = 16.694	v_x = 0.256 v_y = 0.171
MoS_2	C_{11} = 136.261 C_{22} = 136.260	Y_x = 128.178 Y_y = 128.177	Y_y = 51.754	v_x = 0.244 v_y = 0.244

	C_{12} = 33.188 C_{66} = 51.754			
NiS_2	C_{11} = 53.541 C_{22} = 51.852 C_{12} = 26.688 C_{66} = 17.692	Y_x = 39.805 Y_y = 38.549	Y_y = 17.692	v_x = 0.515 v_y = 0.498

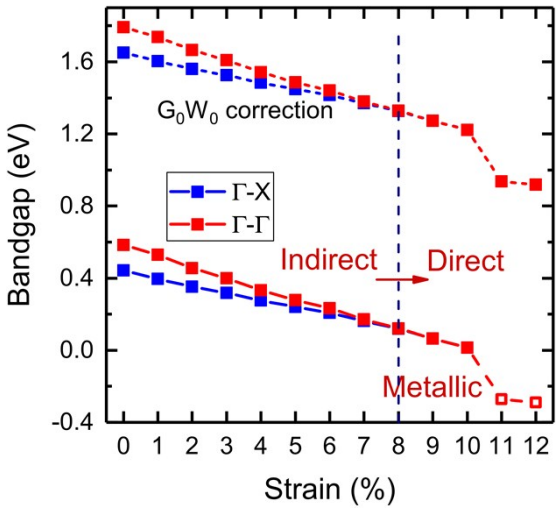

Figure S2. Evolution of the bandgap energy as a function of applied tensile strains (%) within PBE (solid lines) and G_0W_0 correction (dashed lines).

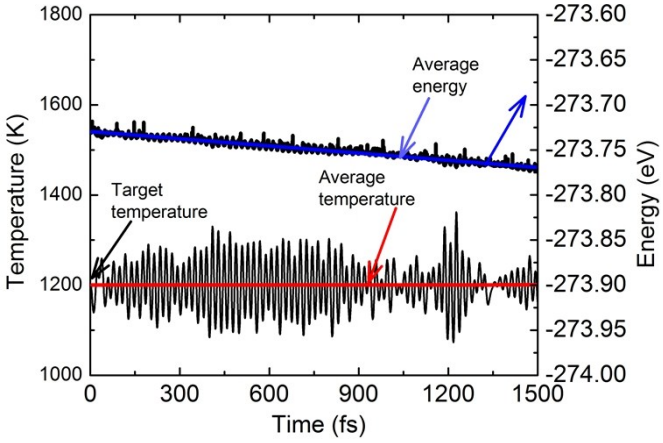

Figure S3. Variation of temperature and the total energy within 1500 fs during AIMD simulation around 1200 K for Ni-MoS_2.

Table S3. Performance of MoS_2, Pt(111) and Ni-MoS_2 catalysts for HER.

Catalyst	ΔG_H (eV)	Optimal condition ($\Delta G_H \approx 0$ eV)	Bandgap (eV)	Water dissociation barrier (eV)

MoS_2	1.736 (present work) ~2[17]	strain and S vacancy simultaneously[17]	1.87 (K-K)[18]	3.2[19]
Pt(111)	~0[20]		Metal	1.07[21]
Ni-MoS_2	0.545	11% strain or 2.5% S vacancy	0.443 (Γ-X)	1.114 (perfect); 0.866 (defective);

References

[1] W. Kohn, L. J. Sham, Phys. Rev., 1965, **140**, A1133-1138.

[2] G. Kresse, J. Furthmüller, Phys. Rev. B, 1996, **54**, 11169-11186.

[3] G. Kresse, J. Furthmüller, Comp. Mater. Sci., 1996, **6**, 15-50.

[4] P. E. Blöchl, Phys. Rev. B, 1994, **50**, 17953-17979.

[5] G. Kresse, D. Joubert, Phys. Rev. B, 1999, **59**, 1758-1775.

[6] J. P. Perdew, K. Burke, M. Ernzerhof, Phys. Rev. Lett., 1996, **77**, 3865-3868.

[7] M. Dion, H. Rydberg, E. Schröder, D. C. Langreth, B. I. Lundqvist, Phys. Rev. Lett., 2004, **92**, 246401-246405.

[8] L. Kong, G. Román-Pérez, J. M. Soler, Phys. Rev. Lett., 2009, **103**, 096103-096107.

[9] K. Lee, É. D. Murray, L. Kong, B. I. Lundqvist, D. C. Langreth, Phys. Rev. B, 2010, **82**, 081101-081105.

[10] J. Klimeš, D. R. Bowler, A. Michaelides, Phys. Rev. B, 2011, **83**, 195131-195144.

[11] G. Henkelman, B. P. Uberuaga, H. Jónsson, J. Chem. Phys., 2000, **113**, 9901-9904.

[12] A. Togo, F. Oba, Isao. Tanaka, Phys. Rev. B, 2008, **78**, 134106-134115.

[13] M. Shishkin, G. Kresse, Phys. Rev. B, 2006, **74**, 035101-035114.

[14] J. K. Nørskov, T. Bligaard, A. Logadottir, J. R. Kitchin, J. G. Chen, S. Pandelov, U. Stimming, J. Electrochem. Soc., 2005, **152**, J23-26.

[15] K. D. Bronsema, J. L. De Boer, F. Jellinek, Z. Anorg. Allg. Chem., 1986, **540**, 15-17.

[16] C. Ataca, H. Şahin, S. Ciraci, J. Phys. Chem. C, 2012, **116**, 8983-8999.

[17] H. Li, *et al*., Nat. Mater., 2016, **15**, 48-53.

[18] C. Ataca, H. Şahin, and S. Ciraci, J. Phys. Chem. C, 2012, **116**, 8983-8999.

[19] B. Tang, *et al*., J. Mater. Chem. A, 2019, **7**, 13339-13346.

[20] J. Greeley, I. E. Stephens, A. S. Bondarenko, T. P. Johansson, H. A. Hansen, T. F. Jaramillo, J. Rossmeisl, I. Chorkendorff, J. K. Nørskov, Nat. Chem., 2009, **1**, 552-556.

[21] J. L. Fajín, M. D. Cordeiro, J. R. Gomes, J. Phys. Chem. A, 2014, **118**, 5832-5840.